

RSC Advances

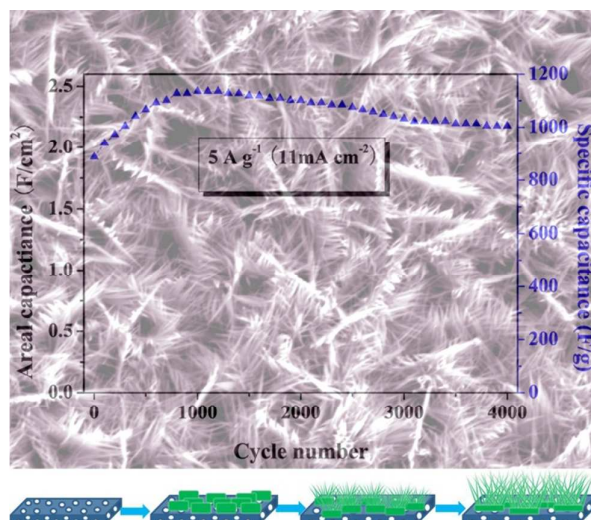


This is an *Accepted Manuscript*, which has been through the Royal Society of Chemistry peer review process and has been accepted for publication.

Accepted Manuscripts are published online shortly after acceptance, before technical editing, formatting and proof reading. Using this free service, authors can make their results available to the community, in citable form, before we publish the edited article. This *Accepted Manuscript* will be replaced by the edited, formatted and paginated article as soon as this is available.

You can find more information about *Accepted Manuscripts* in the [Information for Authors](#).

Please note that technical editing may introduce minor changes to the text and/or graphics, which may alter content. The journal's standard [Terms & Conditions](#) and the [Ethical guidelines](#) still apply. In no event shall the Royal Society of Chemistry be held responsible for any errors or omissions in this *Accepted Manuscript* or any consequences arising from the use of any information it contains.



A novel hierarchical porous NiCo₂O₄ nanograss arrays directly grown on Ni foam has been constructed *via* a simple one-step hydrothermal method combined with a calcination treatment, which possessed high electrochemical performance.

Hierarchical porous NiCo₂O₄ nanograss arrays grown on Ni foam as electrode material for high-performance supercapacitors

Cite this: DOI: 10.1039/x0xx00000x

Received 00th January 2012,
Accepted 00th January 2012

DOI: 10.1039/x0xx00000x

www.rsc.org/

Zhenyu Wang, Yuefei Zhang,* Yonghe Li, Haoyu Fu

A novel hierarchical porous NiCo₂O₄ nanograss arrays directly grown on Ni foam is successfully synthesized through a facile hydrothermal method combined with a thermal treatment. When used as the electrode material for supercapacitor, an areal capacitance of 2.1 F cm⁻² was obtained under the current density of 2 mA cm⁻². After 4000 charge-discharge cycles, the high areal capacitance retention of 94% could be achieved. The outstanding electrochemical performance was attributed to novel structure of hierarchical porous NiCo₂O₄ nanograss arrays and the Ni foam offered as the current collector. The novel hierarchical porous NiCo₂O₄ nanograss arrays would be a promising electrode material for supercapacitors.

Introduction

To meet the increasing demand for energy, tremendous research efforts have been made to develop clean and renewable energy sources.¹⁻⁵ In recent years, supercapacitors, also called electrochemical capacitors or ultracapacitors, have attracted considerable interest as energy-storage devices due to the advantages of high power density, fast charge-discharge process and long life span.^{3,6,7} According to the energy storage mechanism, supercapacitors can be classified into two types, the electrical double-layer capacitors dominated by electrostatic charge diffusion and accumulation at the interface of the electrode/electrolyte, and the pseudocapacitors governed by Faradaic reactions at the surface of electrode materials. Comparing with conventional energy-storage devices, supercapacitors possess quite a few desirable properties, including charging within seconds, long-term cycling stability and the ability to deliver up to ten times more power than batteries. These features are desirable for a range of applications.

Many materials have been investigated as electrode materials for supercapacitors, including carbon-based materials,⁷⁻¹⁰ conducting polymers,^{11, 12} and both noble and transition metal oxides.¹³⁻¹⁷ Transition metal oxides such as NiO,¹⁸⁻²⁰ Fe₂O₃,²¹ CuO,²² MnO₂,^{23, 24} Co₃O₄,^{25, 26} Ni_xCo_{3-x}O₄ (0 < x < 3)²⁷⁻³¹ have attracted tremendous research interest due to the low cost, high

energy density, and environmental friendliness. Among the explored materials for supercapacitors, the ternary nickel cobaltite (NiCo₂O₄) has been investigated as one of the most promising candidates. Comparing with binary nickel oxide (NiO) and cobaltous oxide (Co₃O₄), the ternary nickel cobaltite (NiCo₂O₄) possesses higher theoretical capacity, better conductivity and electrochemical activity.^{27, 32} In recent years, establishment of intriguing architectures for supercapacitor electrode is considered as a necessary factor to boost the electrochemical performance. Furthermore, the method of growing nanostructures on various conductive substrate to fabricate binder-free integrated electrodes for supercapacitors could solve the "dead surface" problems.^{15, 27, 32, 33} Therefore, the NiCo₂O₄ binder-free integrated electrode would have a promising application for supercapacitors.

In this report, a novel hierarchical porous NiCo₂O₄ nanograss arrays directly grown on Ni foam is synthesized via a facile one-step hydrothermal method combined with a post thermal treatment, which can be fabricated as a binder-free electrode for supercapacitors. Such integrated electrode exhibits a high areal capacitance and excellent cycling stability even at a high charge/discharge current density.

Experimental

The porous NiCo_2O_4 nanoglass arrays were fabricated aligned on the Ni foam via a one-step hydrothermal method combined with a post thermal treatment. The reagents used in the experiment were of analytical grade and used without further purification. The Ni foam was carefully cleaned by 3 M HCl in order to remove the NiO layer, and then washed thoroughly with deionized water and absolute ethanol for 20 min each. In a typical procedure^{34, 35}, 0.384 g of $\text{Co}(\text{NO}_3)_2 \cdot 6\text{H}_2\text{O}$, 0.192 g of $\text{Ni}(\text{NO}_3)_2 \cdot 6\text{H}_2\text{O}$ and 1.204 g of urea, 0.296 g of NH_4F were dissolved in 40 ml of deionized water and stirred to form a homogeneous pink solution. Then the aqueous solution and the Ni foam ($1 \times 2 \text{ cm}^2$ in area, the top of the Ni foam about $1 \times 1 \text{ cm}^2$ in area was protected from solution contamination by uniformly coating the top with a polytetrafluoroethylene tape) were transferred to a 50 ml Teflon-lined stainless autoclave, and maintained at $120 \text{ }^\circ\text{C}$ for 6 h. After it was cooled down to room temperature, the red thin product on Ni foam was obtained and subsequently washed with deionized water, ethanol for 5 minutes respectively, and dried at $80 \text{ }^\circ\text{C}$ for 6 h, then calcined at $300 \text{ }^\circ\text{C}$ in air for 2 h.

To address and confirm the characterization of NiCo_2O_4 , the structure of the synthesized products were examined by X-ray diffraction (XRD; Bruker D8 discover) with Cu K α radiation ($\lambda=0.154 \text{ nm}$). The morphology and particles size were observed by scanning electron microscopy (SEM; FEI, Quanta 250), transmission electron microscopy (TEM; JEOL, JEM-2010) equipped with an energy-dispersive X-ray spectroscopy (EDS) system, high resolution transmission electron microscope (HRTEM; JEOL, JEM-2010 F). To calculate the mass loading on the Ni foam accurately, the ICP atomic emission spectrometer (ICP-AES) was applied in the experiment (ESI[†]).

A typical three-electrode cell (equipped with a working electrode, a platinum foil counter electrode, and a Hg/HgO electrode as the reference electrode) was used for measuring the electrochemical properties of the working electrode. And the electrochemical measurements were carried out in 6 M KOH electrolyte. The cyclic voltammetry (CV) and electrochemical impedance spectroscopy (EIS) were studied on an electrochemical workstation (PARSTAT, 2273), galvanostatic charge-discharge (GCD) was tested by Land (LandCT-2001A). Areal and specific capacitances were calculated using equation (1) and (2), respectively.

$$C_a = I \times \Delta t / (S \times \Delta V) \quad (1)$$

$$C_{sp} = I \times \Delta t / (m \times \Delta V) \quad (2)$$

where I (mA) represents the constant discharge current, m (mg), ΔV (V) and Δt (s) designate the mass loading of active materials, potential drop during discharge and total discharge time, respectively. S is the active area of the electrode.

Results and discussion

Morphology and structural analysis

The scanning electron microscope (SEM) images of hierarchical porous NiCo_2O_4 nanoglass arrays are shown in Fig. 1. As can be seen, the nanoglass arrays are uniformly grown on the skeleton of Ni foam (Fig. 1a, b). The higher magnification SEM images (Fig. 1c, d) show that the products exhibit grass-like structure with the surface consists of many needlelike nanowires grown on the nanosheets of below. Furthermore, the nanosheets connect each other and grow aligned on the substrate. And a cluster of hierarchical porous NiCo_2O_4 nanoglass array is about $2 \times 2 \mu\text{m}^2$. The average length and diameter of the surface nanowires is about $2 \mu\text{m}$ and $50\text{-}100 \text{ nm}$ respectively. It is expected that the special structure might have large surface area and high capacitance due to the hierarchical nanoglass

arrays, which would facilitate the access of electrolytes to active material of the electrode.

The transmission electron microscopy (TEM) images are shown in Fig. 2, which demonstrate the microstructures information about NiCo_2O_4 . Fig. 2a shows the full view of a single hierarchical

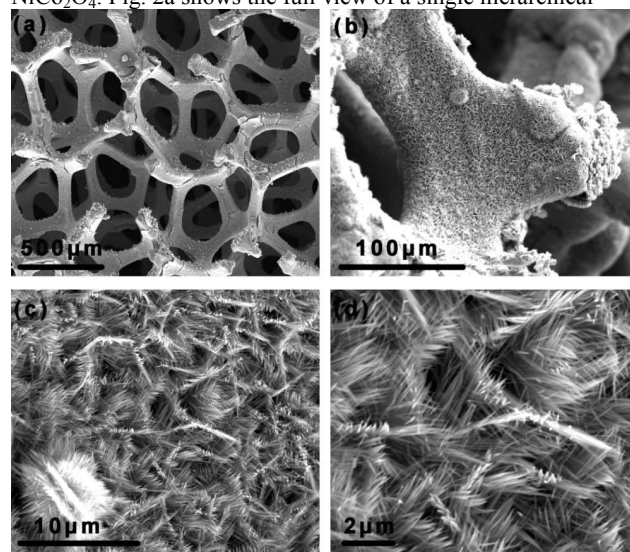


Fig. 1 SEM images of hierarchical porous NiCo_2O_4 nanoglass arrays on Ni foam.

porous NiCo_2O_4 nanoglass array. As can be seen, the nanoglass array consists of nanosheet below and nanowires grown on the nanosheet. A typical selected-area electron diffraction (SAED) pattern (inset of a) is used to indicate the polycrystalline structure of the NiCo_2O_4 nanoglass, the well-defined diffraction rings can be readily indexed to the (111), (200), (220), (311), and (400), which is consistent with the XRD results (Fig. S1, ESI[†]). Fig. 2b reveals that an individual NiCo_2O_4 nanowire consists of numerous interconnected nanoparticles forming a porous structure. The crystalline NiCo_2O_4 nanoparticles have a size of 10 nm in diameter.

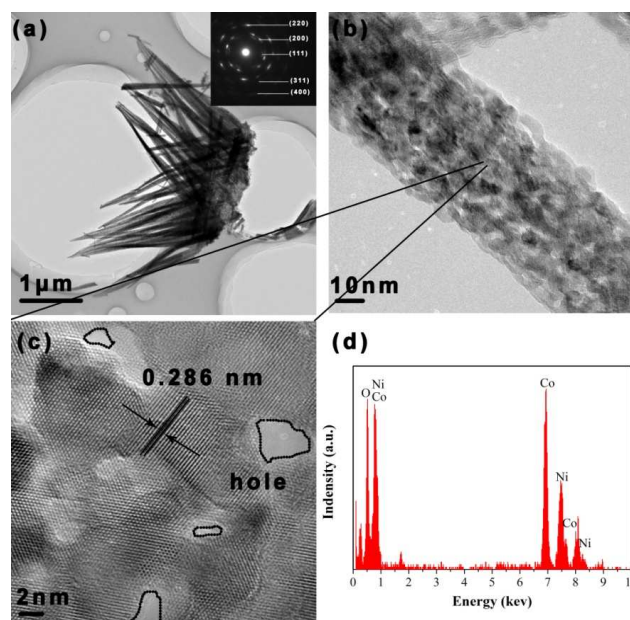


Fig. 2 (a) and (b) TEM images of hierarchical porous NiCo_2O_4 nanoglass arrays. Inset shows the SAED pattern; (c) HRTEM images of NiCo_2O_4 nanowire of b; (d) EDS result of the nanoglass arrays.

Fig. 2c shows the corresponding HRTEM image of the selected area marked in Fig. 2b, which shows the lattice fringes with interplane spacings of 0.286 nm, corresponding to the (220) plane of spinel NiCo_2O_4 material. Furthermore, the nanopores can be seen in the inter-particle with a size of 1-5 nm, which will facilitate the electrolyte transport and contact with the active material. The corresponding result of EDS microanalysis is shown in Fig. 2d. It is found that the nanograss consists of Ni, Co, and O elements, indicating the formation of pure NiCo_2O_4 further.

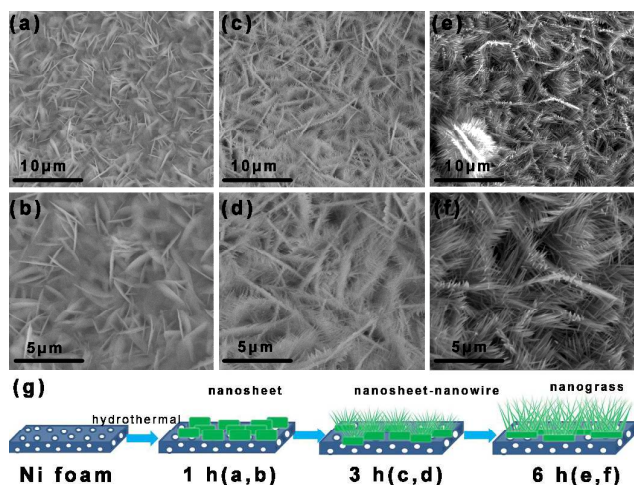


Fig. 3 evolution details of the hierarchical porous NiCo_2O_4 nanograss arrays at different reaction stages. (a) and (b) 1h; (c) and (d) 3 h; (e) and (f) 6 h; (g) schematic illustration of the evolution of hierarchical porous NiCo_2O_4 nanograss arrays on Ni foam.

Synthesis and structural analysis

To explore the evolution details of the hierarchical porous NiCo_2O_4 nanograss arrays on Ni foam, SEM characterization was performed at different reaction stages, as shown in Fig. 3. After reaction for 1 h, the Ni foam was uniformly covered with a layer of nanosheets. However, with further increasing reaction time, after about 3 hours, the morphology changed, nanowires with the length of 0.5-1 μm grown vertically on the nanosheets, which could be imagined the grass grew from the earth. After about 6 hours, the nanowires had grown longer with the length of 2 μm , which formed the main nanograss morphology. Furthermore, it can be seen that the nanograss was supported uniformly on the Ni foam and interconnected with each other, forming an intricate network system, which could enhance the ions transmission efficiency and the electronic conductivity of electrode.

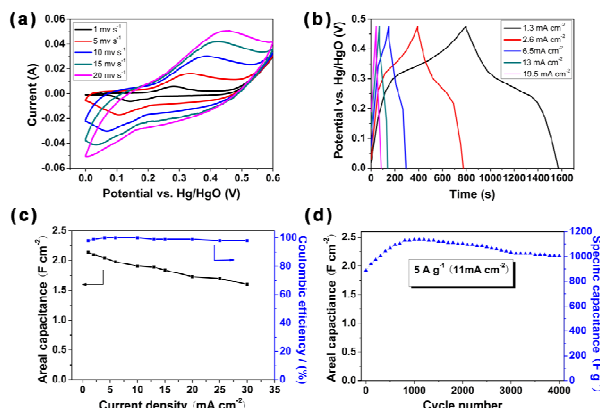


Fig. 4 (a) CV curves at various scan rates; (b) Discharge plots at different current densities; (c) Areal capacitance retention rate as a function of the current density and the coulombic efficiency; (d) Cycling performance of the electrode.

Fig. 4 shows electrochemical performance of the hierarchical porous NiCo_2O_4 nanograss arrays supported on Ni foam. Fig. 4a presents the typical cyclic voltammetry (CV) curves of hierarchical porous NiCo_2O_4 nanograss arrays in a 6 M KOH electrolyte at various scan rates ranging from 1 to 20 mV s^{-1} . The shape of the CV curves clearly reveal the pseudocapacitive characteristics derived from Faradaic reactions. Specifically, two typical redox peaks are observed in the CV curves, which is mainly attributed to the Faradaic redox reactions related to M-O/M-O-OH (M represents Ni or Co) associated with OH anions. The redox reactions in the alkaline electrolyte are expressed as follows,^{27, 28, 32}



Apparently, with the 20-fold increase in the sweep rate from 1 to 20 mV s^{-1} , the current density increases simultaneously, and all curves exhibit a similar shape without obvious polarization, revealing the Ni foam substrate could ensure the good electric conductivity of the electrode, which is verified by the EIS measurement (Fig. S2, ESI†).

Galvanostatic charge-discharge (GCD) measurements were carried out in a 6 M KOH electrolyte between 0 and 0.475 V (vs. Hg/HgO) at various current densities ranging from 1.3 to 19.5 mA cm^{-2} , as shown in Fig. 4b. The voltage plateaus at around 0.3 V in the GCD curves indicate the existence of faradaic processes, which is consistent with the CV curves. With the increasing of current density, the GCD curves still hold excellent symmetry, without obvious IR drop, indicating the outstanding electrochemical reversibility.

To further evaluate the application potential of the hybrid structure as an electrode for supercapacitors, the rate capability and coulombic efficiency have been tested. The areal capacitance (the capacitance per unit area) and specific capacitance (the capacitance per unit mass) calculated by equation (1) and (2) of the experiment section. Encouragingly, the hierarchical porous NiCo_2O_4 nanograss arrays electrode exhibits excellent performance of rate capability with the areal capacitance of 2.14, 2.1, 2.04, 1.98, 1.91, 1.89, 1.84, 1.73, 1.7, 1.6 F cm^{-2} (972, 954, 927, 900, 868, 859, 836, 786, 772, 727 F g^{-1}) at various current densities of 1, 2, 4, 5, 6, 10, 13, 15, 20, 25, 30 mA cm^{-2} respectively. This suggests that about 74.7% of the areal capacitance is still retained when the charge-discharge rate is increased from 1 to 30 mA cm^{-2} . These results are remarkable compared to the previously reported values NiCo_2O_4 -based electrodes. For example, Wang and co-workers obtained a specific capacitance of 294 F g^{-1} at a low discharge current density of 1 A g^{-1} for NiCo_2O_4 nanoplates electrode,³⁷ Tu and co-workers developed the porous NiCo_2O_4 hetero-structure array and obtained a specific capacitance of 891 F g^{-1} at a discharge current density of 1 A g^{-1} ,³⁸ Li and co-workers demonstrated a simple and scalable strategy for synthesizing hierarchical porous NiCo_2O_4 nanowires which exhibited a high specific capacitance of 743 F g^{-1} at 1 A g^{-1} .³⁹ Furthermore, the coulombic efficiency keep nearly 100% all the way.

In addition, Fig. 4d shows the long-term cycling stability of hierarchical porous NiCo_2O_4 nanograss array electrode, which was evaluated by the repeated charging/discharging measurement at a constant current densities of 11 mA cm^{-2} . It can be observed that the area capacitance of the NiCo_2O_4 nanograss arrays electrode increases

gradually in the first 1000 cycles, which can be attributed to the activation of the electrode, which is consistent with some others' results.^{27,37,38} The areal capacitance of the electrode reach the peak value of 2.5 F cm^{-2} (1136 F g^{-1}) at a cycle number of 1000. Afterwards, the areal capacitance begins to decline slowly, which is mainly due to the loss of active material and electrical contact caused by the mechanical stress between the NiCo_2O_4 nanoglass and Nickel foam.⁴⁰ In the end, the areal capacitance of the electrode still has the value of 2.2 F cm^{-2} (1000 F g^{-1}) after 4000 cycles, keeping 88% of the peak value, 113% of the pristine value. The enhanced ion diffusion and effective electron transfer in the hierarchical porous NiCo_2O_4 nanoglass arrays after 1000 cycles are further confirmed by the EIS measurements (Fig. S2, ESI†).^{37,38} The cycling stability of the hierarchical porous NiCo_2O_4 nanoglass arrays electrode is competitive with other NiCo_2O_4 -based nanostructures, such as single-crystalline NiCo_2O_4 nanoneedle arrays, which has 12% loss after 2000 cycles at 5.56 mA cm^{-2} ,³⁴ the ultrathin mesoporous NiCo_2O_4 nanosheets electrode, which has 6% loss at 2 A g^{-1} after 2300 cycles.³² The results demonstrate the outstanding cycling stability of hierarchical porous NiCo_2O_4 nanoglass arrays electrode.

The excellent electrochemical performance of the material is mainly contributed by several factors. First, the Ni foam substrate supports the 3D skeleton for the material to adhere, which not only enhance the stable of the material, but also improve the electrical conductivity of electrode.^{14, 30} Second, the unique structure of hierarchical porous NiCo_2O_4 nanoglass arrays. The nanosheets of the nanoglass connect each other, forming a network, and providing the template for the nanowire to grow, which could enhance the electric contact with the current collector and the utilization of the active material. Third, the novel structure of nanoglass enhances the contact areal between the active material and the electrolyte and improves the electrochemical activity of the material.

Conclusions

In summary, hierarchical porous NiCo_2O_4 nanoglass arrays on Ni foam have been successfully synthesized via a facile hydrothermal method combined a subsequent calcination treatment. The hierarchical porous NiCo_2O_4 nanoglass arrays electrode demonstrate the areal capacitance as high as 2.5 F cm^{-2} (1136 F g^{-1}) at 11 mA cm^{-2} (5 A g^{-1}). In addition, even after more than 4 000 cycles at a high current density, a capacitance of 2.2 F cm^{-2} (1000 F g^{-1}) at 11 mA cm^{-2} with 88.0% retention is achieved. This unique hierarchical array highlights the advantage of NiCo_2O_4 , which demonstrate the outstanding capacitive behavior. So it possess a great promise for the application as supercapacitor electrode.

Acknowledgements

This work was supported by the Beijing Natural Science Foundation (2132014) and the Beijing University of Technology Basic Research Foundation (X4102001201101).

Notes and references

Institute of Microstructure and Property of Advanced Materials, Beijing University of Technology, Beijing, 100124, P. R. China.

E-mail: yfzhang@bjut.edu.cn

† Electronic Supplementary Information (ESI) available: XRD analysis, EIS spectrum.

1. A. S. Arico, P. Bruce, B. Scrosati, J. M. Tarascon and W. Van Schalkwijk, *Nat. Mater.*, 2005, **4**, 366.
2. M. Armand and J. M. Tarascon, *Nature*, 2008, **451**, 652.
3. T. Brezesinski, J. Wang, S. H. Tolbert and B. Dunn, *Nat. Mater.*, 2010, **9**, 146.
4. P. G. Bruce, B. Scrosati and J.-M. Tarascon, *Angew. Chem., Int. Ed.*, 2008, **47**, 2930.
5. C. Yuan, H. B. Wu, Y. Xie and X. W. Lou, *Angew. Chem., Int. Ed.*, 2014, **53**, 1488.
6. P. Simon and Y. Gogotsi, *Nat. Mater.*, 2008, **7**, 845.
7. D.-W. Wang, F. Li, M. Liu, G. Q. Lu and H.-M. Cheng, *Angew. Chem., Int. Ed.*, 2008, **47**, 373.
8. L. L. Zhang and X. S. Zhao, *Chem. Soc. Rev.*, 2009, **38**, 2520.
9. E. Raymundo-Pinero, F. Leroux and F. Beguin, *Adv. Mater.*, 2006, **18**, 1877.
10. D. Y. Qu, *J. Power Sources*, 2002, **109**, 403.
11. G. A. Snook, P. Kao and A. S. Best, *J. Power Sources*, 2011, **196**, 1.
12. X. Wang, N. Li, L. Zheng and Q. Chen, *Prog. Chem.*, 2009, **21**, 1832.
13. W. C. Fang, O. Chyan, C. L. Sun, C. T. Wu, C. P. Chen, K. H. Chen, L. C. Chen and J. H. Huang, *Electrochem. Commun.*, 2007, **9**, 239.
14. L. Bao, J. Zang and X. Li, *Nano Lett.*, 2011, **11**, 1215.
15. J. Liu, J. Jiang, C. Cheng, H. Li, J. Zhang, H. Gong and H. J. Fan, *Adv. Mater.*, 2011, **23**, 2076.
16. Y. Li, P. Hasin and Y. Wu, *Adv. Mater.*, 2010, **22**, 1926.
17. R. Li, X. Ren, F. Zhang, C. Du and J. Liu, *Chem. Commun.*, 2012, **48**, 5010.
18. S. J. Ding, T. Zhu, J. S. Chen, Z. Y. Wang, C. L. Yuan and X. W. Lou, *J. Mater. Chem.*, 2011, **21**, 6602.
19. W. T. Deng, Y. Liu, Y. Zhang, F. Lu, Q. Y. Chen and X. B. Ji, *RSC Adv.*, 2012, **2**, 1743.
20. C. Y. Cao, W. Guo, Z. M. Cui, W. G. Song and W. Cai, *J. Mater. Chem.*, 2011, **21**, 3204.
21. Z. Wang, C. Y. Ma, H. L. Wang, Z. H. Liu and Z. P. Hao, *J. Alloys Compd.*, 2013, **552**, 486.
22. J. S. Shaikh, R. C. Pawar, R. S. Devan, Y. R. Ma, P. P. Salvi, S. S. Kolekar and P. S. Patil, *Electrochim. Acta*, 2011, **56**, 2127.
23. X. H. Li, G. Y. Wang, X. W. Wang, X. P. Li and J. H. Ji, *J. Mater. Chem. A*, 2013, **1**, 10103.
24. Y. Huang, Y. Y. Li, Z. Q. Hu, G. M. Wei, J. L. Guo and J. P. Liu, *J. Mater. Chem. A*, 2013, **1**, 9809.
25. W. W. Zhou, J. P. Liu, T. Chen, K. S. Tan, X. T. Jia, Z. Q. Luo, C. X. Cong, H. P. Yang, C. M. Li and T. Yu, *Phys. Chem. Chem. Phys.*, 2011, **13**, 14462.
26. X. H. Xia, J. P. Tu, Y. J. Mai, X. L. Wang, C. D. Gu and X. B. Zhao, *J. Mater. Chem.*, 2011, **21**, 9319.
27. X. Liu, S. Shi, Q. Xiong, L. Li, Y. Zhang, H. Tang, C. Gu, X. Wang and J. Tu, *ACS Appl Mater Interfaces*, 2013, **5**, 8790.
28. H. Jiang, J. Ma and C. Li, *Chem. Commun.*, 2012, **48**, 4465.
29. L. Yu, G. Q. Zhang, C. Z. Yuan and X. W. Lou, *Chem. Commun.*, 2013, **49**, 137.
30. G. Y. He, L. Wang, H. Q. Chen, X. Q. Sun and X. Wang, *Mater. Lett.*, 2013, **98**, 164.
31. H. B. Wu, H. Pang and X. W. Lou, *Energy Environ. Sci.*, 2013, **6**, 3619.
32. C. Z. Yuan, J. Y. Li, L. R. Hou, X. G. Zhang, L. F. Shen and X. W. Lou, *Adv. Funct. Mater.*, 2012, **22**, 4592.
33. C. Zhou, Y. W. Zhang, Y. Y. Li and J. P. Liu, *Nano Lett.*, 2013, **13**, 2078.
34. G. Q. Zhang, H. B. Wu, H. E. Hoster, M. B. Chan-Park and X. W. Lou, *Energy Environ. Sci.*, 2012, **5**, 9453.
35. G. Zhang and X. W. David Lou, *Sci. Rep.*, 2013, **3**, 1470.
36. Q. Wang, X. Wang, B. Liu, G. Yu, X. Hou, D. Chen and G. Shen, *J. Mater. Chem. A*, 2013, **1**, 2468.
37. J. Pu, J. Wang, X. Jin, F. Cui, E. Sheng and Z. Wang, *Electrochim. Acta*, 2013, **106**, 226.
38. X. Y. Liu, Y. Q. Zhang, X. H. Xia, S. J. Shi, Y. Lu, X. L. Wang, C. D. Gu and J. P. Tu, *J. Power Sources*, 2013, **239**, 157.
39. H. Jiang, J. Ma and C. Li, *Chem. Commun.*, 2012, **48**, 4465.
40. R. Wang, Z. Chen, H. Yu, X. L. Jia, L. Gao, J. Sun, R. F. Hicks and Y. F. Lu, *Nanoscale*, 2014, **6**, 3791.